Brillouin spectroscopy of polarization fluctuations in $Rb_{1-x}(NH_4)_xH_2PO_4$ mixed crystals: Concentration dependence

Eric Courtens, René Vacher,* and Yves Dagorn†
IBM Zurich Research Laboratory, 8803 Rüschlikon, Switzerland
(Received 12 May 1986; revised manuscript received 12 February 1987)

Brillouin-scattering results from modes coupling linearly to the polarization are presented for ammonium concentrations $x=0.15$, 0.20, 0.25, 0.72, 0.75, and 0.78. For the two lowest and two highest concentrations, structural transitions occur on cooling, while the middle two represent both extremes of the range of x for which structural glasses form in this system. In combination with dielectric and birefringence measurements, the following information is extracted from the data: the anharmonicity of the uncoupled acoustic modes, the strength of the piezoelectric coupling, the growth of quasistatic electrostriction effects below $\simeq 100$ K in the glass-forming range, as well as that of dynamic effects also related to electrostriction. The strength of the latter two increases markedly with x. Excellent fits to the Brillouin spectra are obtained with a model of polarization fluctuations that assumes a broad distribution of relaxation times. Various integrals on that distribution are extracted from the spectra. The structural transitions near the glass boundaries of the phase diagram are complex. On the Rb-rich side, unusually strong polarization fluctuations remain below the transition.

I. INTRODUCTION

It is now well established that the isomorphous tetragonal crystals RbH_2PO_4 (RDP) and $NH_4H_2PO_4$ (ADP), both paraelectric (PE) at room temperature, form solid solutions $Rb_{1-x}(NH_4)_xH_2PO_4$ (RADP) that constitute an excellent model system for the investigation of freezing in structural glasses.[1-3] RDP becomes ferroelectric (FE) at $\simeq 146$ K, while ADP transforms to an antiferroelectric (AFE) structure at $\simeq 148$ K.[4] In RADP, the specific hydrogen bonding of the randomly distributed ammonium ions competes with the FE ordering of the acid protons.[5] For intermediate ammonium concentrations x, $0.22 \lesssim x \lesssim 0.74$, this competition forces the disordered acid-proton configurations of the PE phase to freeze into a glass on cooling.[6] In that case, the average crystal point group remains unchanged down to liquid-He temperatures.[7,2] Outside this range of x, structural transitions towards phases of lower symmetries occur.[1,2] Those phases resemble somewhat the FE phase on the Rb-rich side, and the AFE one on the NH_4-rich side, respectively, but can be more complicated near the glass-phase boundaries.[8]

The glass state of RADP can be described by randomly frozen local polarizations.[1] In crystals of the KH_2PO_4 (KDP) family, the polarization is both linearly and quadratically coupled to strains.[4] Hence, considerable information on freezing can be gained with Brillouin spectroscopy of the acoustic modes.[9] It was shown in Ref. 10, hereafter referred to as I, that combined dielectric and Brillouin-scattering measurements from piezoelectrically coupled modes can be described consistently in terms of the development of a broad temperature-dependent distribution $g(\tau,T)$ of relaxation times τ, below an onset of freezing at $\simeq 100$ K. A consequence of the distribution on the light-scattering spectra is the simultaneous presence of a dynamical central peak and of a polarization-fluctuation induced broadening in the Brillouin lines.[10] The resulting spectral profiles, together with the dielectric data, could be interpreted fully coherently with this model. Recently, it was pointed out in Ref. 11, hereafter referred to as II, that the data analysis could conveniently be made in terms of an expansion of a relaxation function κ in the logarithm of the frequency ω,

$$\kappa(\omega,T)\equiv\kappa_R+i\kappa_I=\int_{-\infty}^{\infty}\frac{g(\tau,T)d\ln\tau}{1-i\omega\tau}\ . \tag{1}$$

Glass fluctuations, on the other hand, have been observed on acoustic modes coupled to the polarization by electrostriction.[12] Those studies were performed for the particular concentration $x=0.35$.

In the present paper, dielectric and Brillouin-scattering results on the modes observed in I are presented, but covering a broad range of concentrations, three Rb-rich ($x=0.15$, 0.20, and 0.25), and three NH_4-rich ($x=0.72$, 0.75, and 0.78) ones. For the two lowest and two highest values of x, transitions do actually occur, while the middle values are characteristic of either extreme in the glass-composition range. The long-wavelength polarization fluctuations seen in light scattering are dominant on the RDP side, while they become relatively weak on the ADP side. This is not so, however, for the *glass* fluctuations, which relate to changes in local AFE order as well as to changes in local FE order. We also show that Brillouin measurements can be performed below the PE to ordered phase transitions. On the FE side, close to the glass boundary, those measurements reveal a considerable amount of disorder that remains dynamical down to very low temperatures in the so-called ordered phase.

The paper is subdivided as follows. In Sec. II, x and temperature (T) dependences of the dielectric constants at low and high frequencies are presented. These allow derivation of a coupling constant important to the inter-

pretation of the Brillouin spectra. Section III describes the anharmonic behavior of the birefringence from which Debye temperatures are derived, and that of the bare (not piezoelectrically coupled) acoustic frequencies. The latter are shown to obey a simple interpolation rule, with an anharmonicity essentially x independent. Section IV discusses fits obtained on the two glass-forming concentrations, $x=0.25$ and 0.72, while Sec. V explains the main observations made on crossing the transitions with samples of the four other concentrations. The major results are summarized in Sec. VI.

II. DIELECTRIC MEASUREMENTS

The dielectric constant parallel to the crystallographic c axis (ϵ_c') was determined for all x values used in this study. The concentrations, approximately known from the composition of the crystal-growth solutions, were in each case determined from x-ray lattice-parameter measurements with an absolute accuracy better than 1%.[6] For dielectric measurements, the samples were thin plates cut perpendicular to the c axis to better than 0.5°. They were usually derived from the same single crystals used for the light-scattering experiments, or else from crystals of the same batch. The plates were typically 0.5–1 mm thick with a surface area of 10–20 mm^2. The large faces were gold plated by evaporation after a chromium flash. The edges were finely ground to remove traces of metal. Finally, thin wires were attached with a drop of silver paste.

The capacitance and parallel conductance of those samples were measured with an automated system consisting of a Hewlett Packard HP-4192A impedance analyzer, a Cryodyne CTI 21SC closed-cycle refrigerator, a Lake Shore Cryogenics DRC82C temperature controller, all connected with an IEEE bus to an IBM PC-AT running under APL control software. In this system, the samples are mounted in vacuum to a holder to which they make contact with heat-conducting grease. All wires are heat-sunk to that holder which also supports the calibrated Si-diode thermometer. Measurements are performed point by point: after each temperature change, the system waits until the new value has been reached within a set deviation. It then waits for an additional set delay to achieve good thermalization, and it finally takes a series of measurements of capacitance and conductance at various frequencies. In the present case, the latter were selected in geometric progression, with a dozen of values between 100 Hz and 13 MHz. For c-cut samples, results in the middle of the range (around 100 kHz) are usually strongly perturbed by piezoelectric resonances, while at the lowest frequencies (100–300 Hz) the values are imprecise in view of the small capacitance of our samples (a few picofarads). The measured capacitances are converted into dielectric constants using the sample dimensions. The low-frequency, or free dielectric constant ϵ_{fr} is obtained with highest accuracy from measurements in the 1–10 kHz range, while the high-frequency, or clamped dielectric constant ϵ_{cl} is obtained between 3 and 13 MHz.

Figure 1 shows the low-temperature behavior of ϵ_c' for the compositions on the Rb-rich side. The samples with

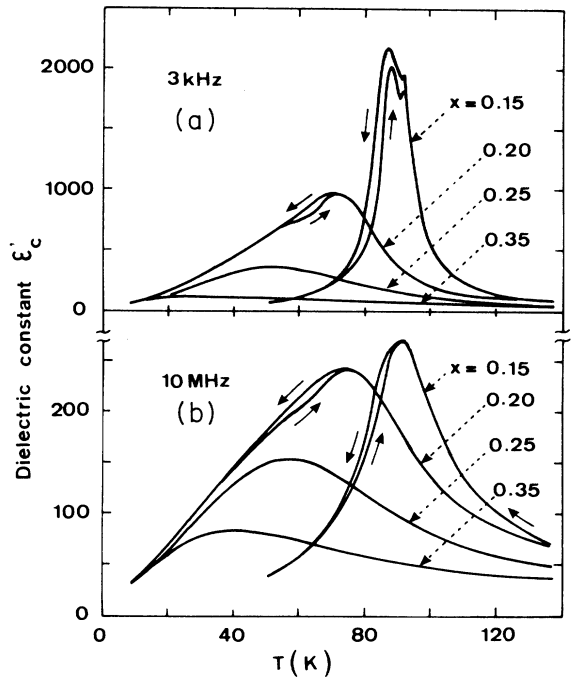

FIG. 1. Dielectric constants ϵ_c' for Rb-rich concentrations: (a) free values, and (b) clamped values. The arrows indicate the measurement direction.

$x=0.15$ and 0.20 clearly reach a high value of ϵ_c' and then make a transition to another phase, associated with hysteresis as seen from the difference between the cooling and heating curves. Those with $x=0.25$ and 0.35 remain in the tetragonal phase. The first sharp peak obtained on cooling the $x=0.15$ sample is at 92 K. For $x=0.20$, transition phenomena have a greater spread, and a cusp is best seen on heating at $\simeq 72$ K. The difference between free and clamped values (3 and 10 MHz, respectively) is largest near the FE-like transitions. The associated low-frequency losses ϵ_c'' (at 1 kHz) have an onset on cooling at ~ 85, 75, 52, and 30 K, with peak values of about 140, 30, 15, and 8, for $x=0.15$, 0.20, 0.25, and 0.35, respectively. All ϵ_c' curves exhibit frequency dispersion at temperatures below their peak in Fig. 1. The dispersion for the $x=0.15$ sample is, however, weaker than for the other compositions.

Dielectric data for compositions on the AFE side are illustrated in Fig. 2. In comparing these curves, one must note that the differences seen at high-T remain within the measurement accuracy of the contact area. The $x=0.72$ sample shows no transition to a new state, while the other two concentrations do exhibit a sharp change associated with hysteresis in the case of $x=0.75$. The dispersion, not shown on Fig. 2, which is practically absent for $x=0.78$, is very weak and occurs below the first-order transition for 0.75, and it is present for $x=0.72$. On the AFE side, the values of ϵ_c' are much smaller than those along the a axis ϵ_a',[13] emphasizing that FE-type fluctuations contribute only weakly at those concentrations.

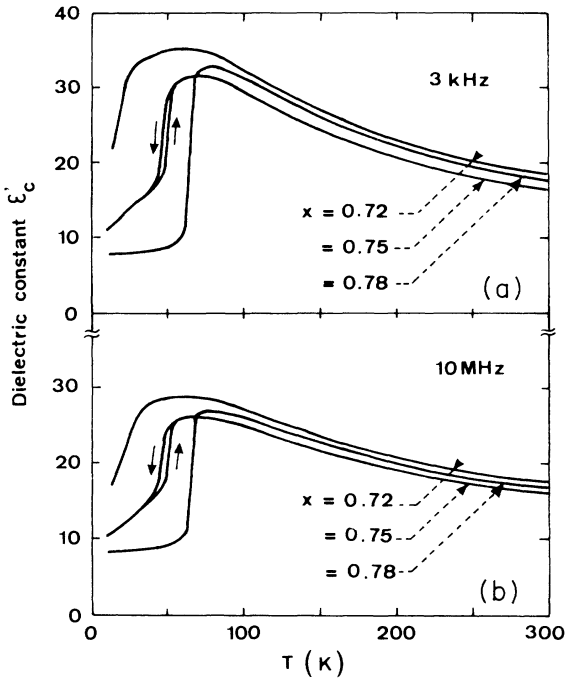

FIG. 2. Dielectric constants ϵ'_c for NH_4-rich concentrations: (a) free values, and (b) clamped values. The arrows indicate the measurement direction.

An inverse coupling constant Q can be extracted from a comparison of the free and clamped dielectric constants, $1/Q=1-(\epsilon_{cl}-1)/(\epsilon_{fr}-1)$, as explained in I. This parameter is useful for the analysis of the light-scattering spectra. Results for three compositions in the glass range are shown in Fig. 3. At low temperatures, the dispersion, which first appears in the 10-MHz data on cooling, prevents the determination of Q, as shown by the dashed part of the curves. On comparing the temperature dependence of Q at $x=0.25$ and 0.72, one notices that the coupling at high temperature is larger (Q is smaller) on the AFE side. This is connected with the larger piezoelectric constant of ADP compared to RDP. At low temperatures, the coupling becomes much stronger on the FE side owing to the large increase of the low-frequency contribution $\chi_0(T)$ to the susceptibility. For $x=0.25$, one notes that the system is rather close to an elastic instability, given the values of Q near to one.

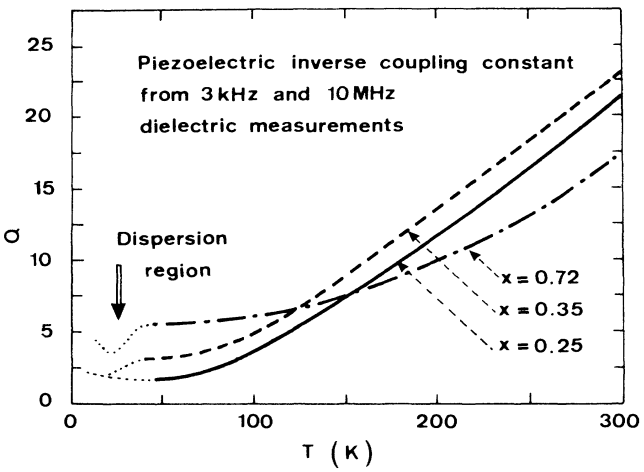

FIG. 3. Constant Q derived from the dielectric measurements for the glass-forming concentrations. The dotted part of the curves is affected by dispersion and cannot be used.

III. LATTICE ANHARMONICITY

To analyze the Brillouin data, it is advantageous to know the anharmonic behavior of the bare acoustic frequencies $\omega_a(T)$. The latter is the phonon frequency decoupled from polarization fluctuations. Its temperature dependence can be described by a Debye function, as shown in I. An appropriate value of the Debye temperature Θ could be obtained from lattice parameter measurements.[7] Alternatively, and more simply, it can also be derived from the natural birefringence of the crystals.[1] On the other hand, the bare phonon frequencies are obtained using

$$\omega_a \cong \omega_B[Q'/(Q'-1)]^{1/2} ,$$

where ω_B is the frequency of the Brillouin peak observed. In that equation, Q' equals the dielectric Q for the transverse acoustic mode $T_1[100]$, hereafter designated by TA. Q' is proportional to Q for the longitudinal acoustic mode $L[110]$, to be designated by LA. The values of ω_B are obtained at high temperatures from Brillouin data. The values $\omega_a(T)$, calculated with Q', are then fitted to a Debye law using the known Θ. These steps are detailed in the following.

A. Birefringence measurements

The temperature dependence of the natural birefringence was measured on the same crystals used for the light-scattering experiments. To this effect, those were placed in the automated closed-cycle refrigerator, and illuminated by a weak ($\simeq 1$ mW), slightly focused laser beam at $\lambda=6328$ Å. The light was polarized in a direction bisecting the **a** and **c** crystallographic axes, and propagated along **b**. The crystal was followed by an analyzer and a photodiode. The computer-controlled measurements proceeded point by point, at typically 0.5-K intervals, each time waiting for thermalization. For each point, the input laser power, the depolarized transmitted signal, and the temperature were recorded. The normalized output signal is approximately a sinusoid whose period corresponds to a retardation increase by λ. The effect of the change of the geometric path length being negligible compared to the birefringence change $\delta(n_0-n_e)=\delta(\Delta n)$, the recorded signal can immediately by analyzed to extract $\delta(\Delta n)$.

The results, including a new curve for $x=0.35$, are shown as solid lines in Fig. 4. The transitions for $x=0.15$ and 0.2 do not prevent the low-temperature measurement. For $T>125$ K, the behavior is completely controlled by lattice anharmonicity, and can be represented by

$$\delta(\Delta n)=\delta(\Delta n)_0-B\Theta F\left[\frac{\Theta}{T}\right] . \quad (2)$$

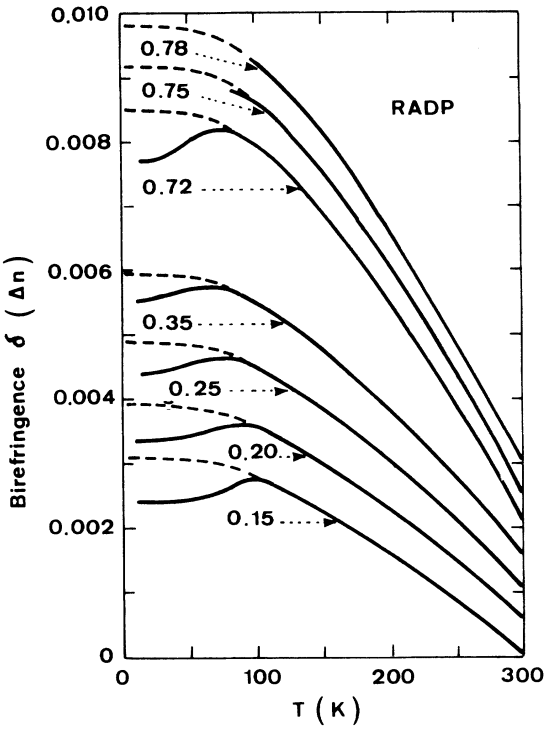

FIG. 4. Birefringence changes at $\lambda=6328$ Å (solid curves), and the extrapolated fits to a Debye free-energy function (dashed curves).

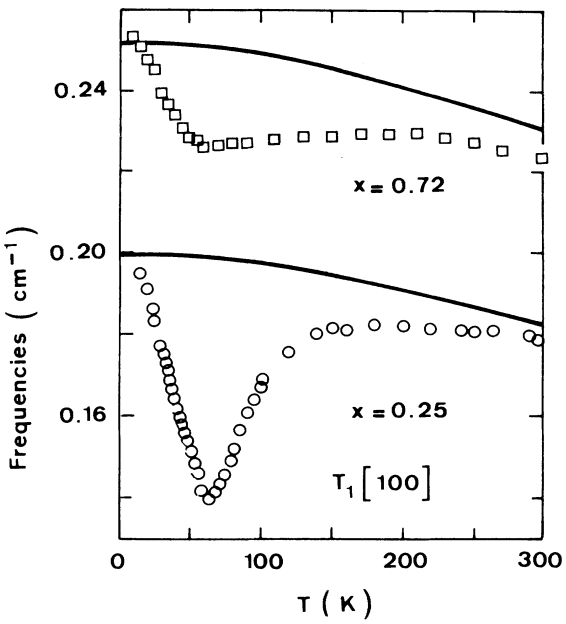

FIG. 5. Frequencies of the TA phonons for $x=0.25$ (lower part) and 0.72 (upper part). The points are the values ω_B from the Lorentzian fits to the Brillouin spectra, while the solid curves are ω_a values as explained in connection with Fig. 6.

where F is the Debye function defined in (8b) of I. Fitting with (2), one finds the values of Θ listed in Table I. One notices that the general tendency is for Θ to increase from the RDP side to the ADP side, as can be expected in view of the higher frequency of the modes in ADP. The low temperature extrapolation of the Debye fits is shown by the dashed curves in Fig. 4. The difference between the lines and the dashed curves is proportional to the square of the internal polarizations.[1]

B. Anharmonicity of the bare frequencies

The TA and LA Brillouin spectra were measured with a laser wavelength $\lambda=5145$ Å, in 90°-scattering geometry, as described in detail in I. The frequencies ω_B of the coupled acoustic modes were extracted by performing Lorentzian fits to the experimental spectra. Such fits are excellent, within our experimental accuracy, on the AFE side, as well as on the FE side for $T>100$ K. At lower T on the FE side, those fits, although not perfect, also give good estimates of the phonon softening. Results for the TA mode at $x=0.25$ and 0.72 are shown in Fig. 5. The solid lines represent the bare frequencies $\omega_a(T)$ obtained as explained below. The difference between ω_a and ω_B above 100 K is larger on the AFE side, in accordance with the stronger piezoelectric coupling discussed in relation with Fig. 3. On the other hand, the minimum around 60 K is deeper for concentrations on the FE side, in view of the larger strength of long-wavelength polarization fluctuations in that case. One notices that at very low temperature, the bare frequency ω_a matches the experimental ω_B within the accuracy.

TABLE I. The Debye temperatures $\Theta(x)$ derived from fits to the birefringence data of Fig. 4.

x	Θ (K)
0.15	423
0.20	399
0.25	406
0.35	417
0.72	470
0.75	484
0.78	483

The determination of the bare TA frequencies for the seven values of x is illustrated in Fig. 6. The points are the ω_a's calculated from the ω_B's using Q. These have been fitted with

$$\omega_a(T,x)=\omega_a(0,x)\left[1-A\Theta(x)F\left[\frac{\Theta(x)}{T}\right]\right], \tag{3}$$

where $\Theta(x)$ was taken from Table I. It is remarkable that fits with A constant, i.e., with the same amount of anharmonicity at all compositions, are rather satisfactory, as illustrated by the solid lines on Fig. 6. For the TA modes, one finds for A, $A_{\mathrm{TA}}=5.12\times10^{-4}$. The corresponding values of $\omega_a(0,x)$ are plotted in Fig. 7, together with the TA frequencies calculated for pure RDP and ADP using data from Ref. 4. A linear dependence on concentration is found. Similar results are obtained for the LA frequencies as illustrated in Fig. 8. In this case one finds

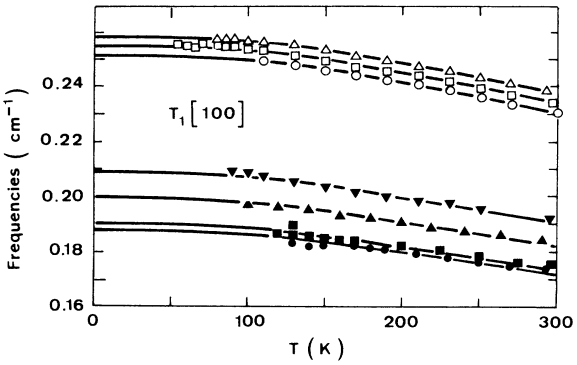

FIG. 6. Bare frequencies ω_a of the TA phonons. The points are calculated from the ω_B values obtained from Lorentzian fits. They are ●, ■, ▲, ▼, ○, □, and △, for $x=0.15$, 0.20, 0.25, 0.35, 0.72, 0.75, and 0.78, respectively. The curves are fits as explained in the text.

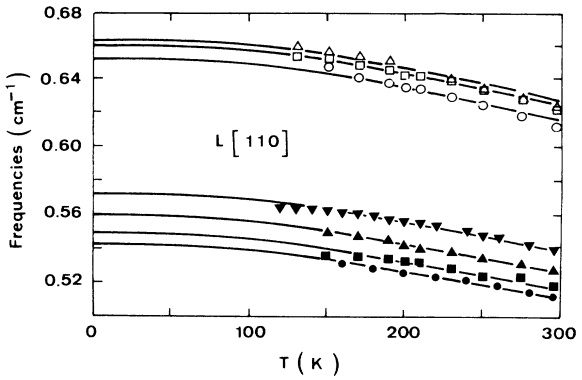

FIG. 8. Bare frequencies ω_a of the LA phonons. The points are calculated from the ω_B values, and the symbols are the same as in Fig. 6. The curves are fits as explained in the text.

$A_L=3.42\times10^{-4}$, and also a linear dependence of $\omega_a(0,x)$ on x (Fig. 7).

From those results, one derives the mode Grüneisen constant γ defined by $d\ln\omega_a=-\gamma d\ln V$, where V is the sample volume. Numerical calculations can be performed for $x=0.35$ and 0.72, since the temperature dependence of the lattice parameters are known at these concentrations.[7,14] The results for $x=0.35$ are $\gamma_{LA}=3.6$ and $\gamma_{TA}=5.1$, for the LA and TA modes, respectively. For $x=0.72$, one finds $\gamma_{LA}=4.0$ and $\gamma_{TA}=5.6$. These relatively large Grüneisen constants are to be related to the great sensitivity of the H bond on pressure. This depends but weakly on concentration. The particularly large γ_{TA} values indicate that the transverse mode frequencies are strongly influenced by hydrogen bonding.

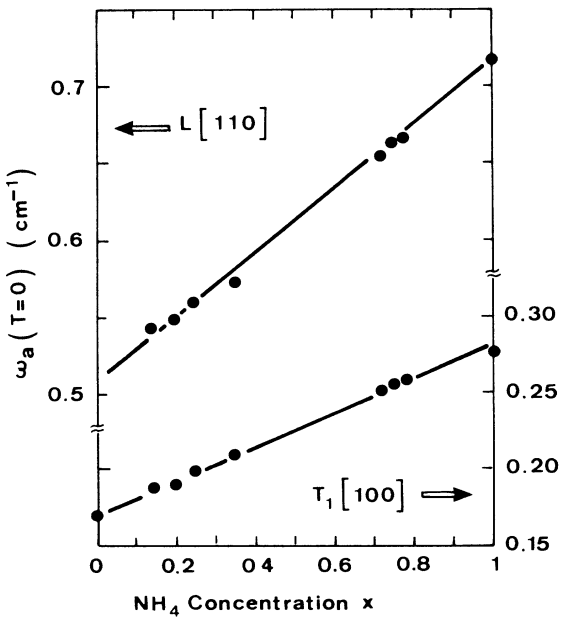

FIG. 7. Zero-temperature bare phonon frequencies $\omega_a(T=0)$ as a function of x for the TA (right scale) and the LA (left scale) modes.

IV. BRILLOUIN SPECTRA ON GLASS-FORMING COMPOSITIONS

To extract reliably the relevant information from the measured Brillouin spectra in the temperature range where polarization and strain strongly couple, it is necessary to fit them with the full spectral profile, as explained in I and II. Since a number of parameters is involved, fits with all parameters free are meaningful only for strongly coupled spectra, as is the case for $x=0.25$ and $50<T<75$ K. Otherwise, best use should be made of the ancilliary information derived in the two preceding sections. The fit strategy and the main results will now be described for the samples at $x=0.25$ and 0.72.

A. T_1[100] spectra

Spectra taken in the temperature range corresponding to the maximum softening were first fitted with Q fixed to its value shown in Fig. 3, and all other parameters free following the approach taken in I. From those results, an average value was derived for the dimensionless and nearly temperature-independent quantity $\Upsilon\equiv aC/ph$. Here, $a\equiv a_{36}$, $p\equiv p_{66}$, and $h\equiv h_{36}$, are the appropriate electrooptic, piezooptic, and piezoelectric coupling coefficients, respectively, while C is the elastic constant for the mode in question. We find $\Upsilon=4$ for $x=0.25$, and $\Upsilon=2$ for $x=0.72$. As Υ has little influence on the profile calculated, its value was then fixed for subsequent fits. Taking the approach of II, Q, and ω_a were fixed as described in the previous sections, while $\kappa_R(\bar\omega,T)$, $\kappa_I(\bar\omega,T)$ and $m(\bar\omega,T)$ were determined by fitting the spectra. Here, $\bar\omega/2\pi=0.10$ cm^{-1} is the mean frequency about which κ is developed in $\ln\omega$. The coefficients $\kappa_R(\bar\omega)$, $\kappa_I(\bar\omega)$, and $m(\bar\omega)$ are essentially those of the development of κ_R in $\ln\omega/\bar\omega$ of order 0, 1, and 2, respectively.[11] This approach gives excellent fits, and the resulting coefficients are shown in Figs. 9 and 10. For $x=0.72$, the spectra are insufficiently coupled to determine m which is then set equal to 0. On the other hand, the $x=0.25$ spectra being

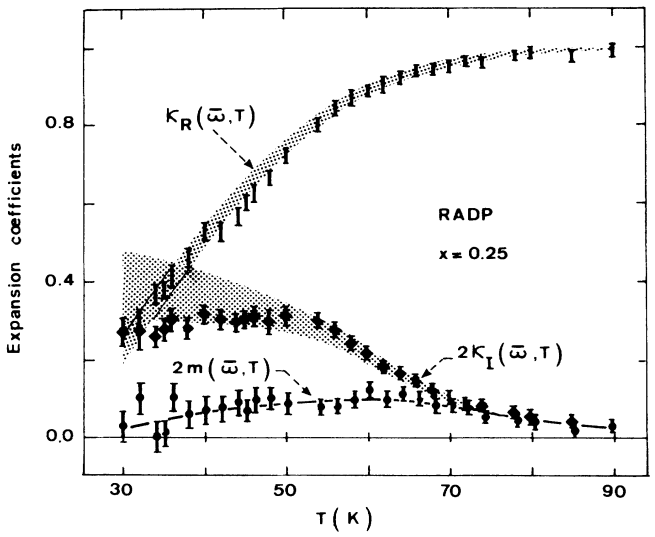

FIG. 9. Expansion coefficients $\kappa_R(\bar{\omega},T)$, $\kappa_I(\bar{\omega},T)$, and $m(\bar{\omega},T)$ for $x=0.25$, with $\bar{\omega}/2\pi=0.10$ cm^{-1}. The shaded areas are self-consistency checks based on a VF assumption with $T_0=14$ K and $\omega_0/2\pi=100$ cm^{-1}, as explained in the text.

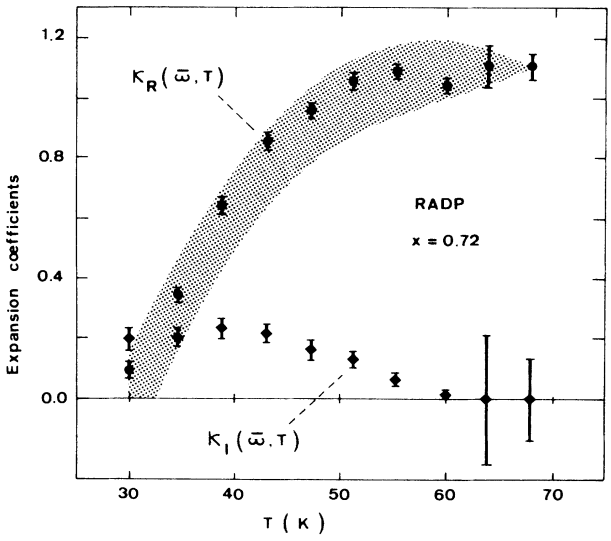

FIG. 10. Same as Fig. 9, for $x=0.72$ and $T_0=21$ K; m was set equal to zero in this case.

strongly coupled, we could verify that their fits with a single Debye relaxation instead of a distribution are very poor. The importance of the distribution is illustrated in Fig. 11 which shows the ratios $\kappa_R/(\kappa_R^2+\kappa_I^2)$ derived from Figs. 9 and 10. As explained in II, the deviation from 1 of these ratios indicates that the distributions of relaxation times acquire appreciable weight at long times $\tau>1/\bar{\omega}$. This occurs below $\simeq 65$ K for $x=0.25$, and below $\simeq 50$ K for $x=0.72$.

The error bars on Figs. 9 and 10 are the estimated standard deviations resulting from the fit statistics. As pointed out in II, systematic errors are Q and ω_a affect the expansion coefficients, particularly $\kappa_R(\bar{\omega})$, but much less the other two. If one assumes, like for $x=0.35$,[3] that $g(\tau,T)$ can be derived from a distribution of energies $f(E)$, where E is related to τ and T by the Vogel-Fulcher law $\tau=\tau_0\exp[E/(T-T_0)]$, the self-consistency of the expansion coefficients can be checked.[11] This check is illustrated by the shaded areas in Figs. 9 and 10. The one around κ_I in Fig. 9 results from the integration of m, using Eq. (7b) of II with $T_0=14$ K, and $1/(2\pi\tau_0)=100$ cm^{-1}. Those around κ_R in Figs. 9 and 10 result from the integration of κ_I, using (7a) of II, with $T_0=14$ K for $x=0.25$ and $T_0=21$ K for $x=0.72$. The self-consistency is remarkable, given that the integrations are performed without any free parameter except the Vogel-Fulcher temperature T_0.

The distribution functions $f(E)$ derived from $\kappa_I(\bar{\omega},T)$ using Eq. (6) of II are shown in Fig. 12. It is remarkable that these distributions automatically normalize to 1 when low-energy cutoffs are assumed, as sketched by the dashed lines in Fig. 12, and as already found for the dielectric data at $x=0.35$.[3] It is also remarkable that the function $f(E)$ obtained in II for $x=0.35$ is intermediate between these two. The higher energy tail at concentrations nearer to the FE boundary is consistent with an earlier departure from 1 on cooling found for the ratio in Fig. 11. Those higher activation energies on the FE side should probably be related to larger FE-type clusters which are more likely to form at small NH_4 concentrations. The reorientation of such clusters can be expected to involve higher energy barriers.

B. *L*[110] spectra

Figure 13 shows the measured ω_B values for the LA modes together with Debye fits to the high temperature values of the bare frequencies ω_a. Striking differences from the corresponding curves for the TA modes (Fig. 5) are seen. Firstly, the measured ω_B do not tend towards the extrapolated Debye value of ω_a at very low tempera-

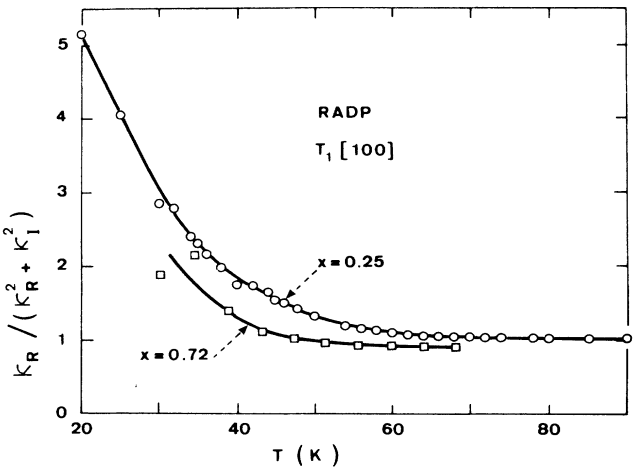

FIG. 11. Ratios $\kappa_R/(\kappa_R^2+\kappa_I^2)$ determined from the coefficients in Figs. 9 and 10. The lines are guides to the eye.

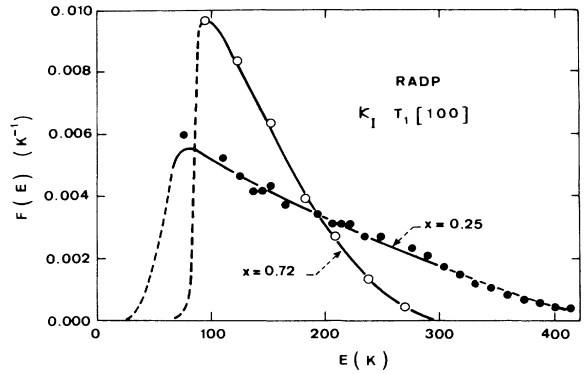

FIG. 12. Distributions of activation energies derived from $\kappa_I(\bar{\omega},T)$ in Figs. 9 and 10. The lines are guides to the eye with an area normalized to one.

tures. Secondly, the depth of the minima around 60 K are now about equal for both concentrations, while the minimum was much deeper on the Rb-rich side than on the NH_4 side in the case of the TA modes.

The fact that the extrapolated Debye frequency value is higher than the experimental LA frequency at very low temperature was already observed for $x=0.35$ in I. It was interpreted as an effect of either very slow or truly frozen polarization fluctuations associated with the development of a glass order parameter. This departure of ω_a from the extrapolated Debye behavior must parallel that of the birefringence which has the same origin.[1] Hence, the bare frequencies ω_a can be approximated by the solid line in Fig. 13, where the difference between solid and dashed lines is proportional to that in Fig. 4, the proportionality factor being such that the low-temperature experimental values fall on the solid curve.

Electrostriction effects, whose existence was demonstrated in a study of the $L[100]$ mode,[12] have been shown to be responsible for about half the LA softening at $x=0.35$ in I. Since the depth of the minima in Fig. 13 is nearly equal at both concentrations, and since the linear piezoelectric coupling at those temperatures is smaller for $x=0.72$ than for 0.25, as seen in Fig. 3, one concludes that the quadratic electrostriction coupling must increase with the NH_4 content. This conjecture is fully supported by the results of the fits explained below.

Typical LA spectra are shown in Fig. 14. For the fits, appropriate values of Υ were calculated from those determined for the TA spectra. One finds $\Upsilon=31$ for $x=0.25$, and $\Upsilon=13.5$ for $x=0.72$. The values of $\kappa_R(\bar{\omega},T)$ and $\kappa_I(\bar{\omega},T)$, at $\bar{\omega}/2\pi=0.3$ cm^{-1}, were taken from the TA spectra, and ω_a was fixed from Fig. 13. Q' and the intensities are now the only adjustable parameters. The results for Q' are shown as Q'_{eff} in Fig. 15. Also shown are the values of Q' calculated from the dielectric data using the known ratio of TA-to-LA elastic constants in $Q'\equiv C/\chi(0,T)h^2$. One sees that $1/Q'_{\text{eff}}$ is significantly larger than $1/Q'$ in both cases. This demonstrates that our results are properly accounted for when one assumes that the combination of piezoelectricity and electrostriction leads to an effective coupling parameter $(Q'_{\text{eff}})^{-1}\simeq 2(Q')^{-1}$ for $x=0.25$, and $(Q'_{\text{eff}})^{-1}\simeq 3.2(Q')^{-1}$ for $x=0.72$. Hence, electrostriction increases with NH_4 content and becomes the dominant coupling mechanism for $x=0.72$, in agreement with the above conjecture.

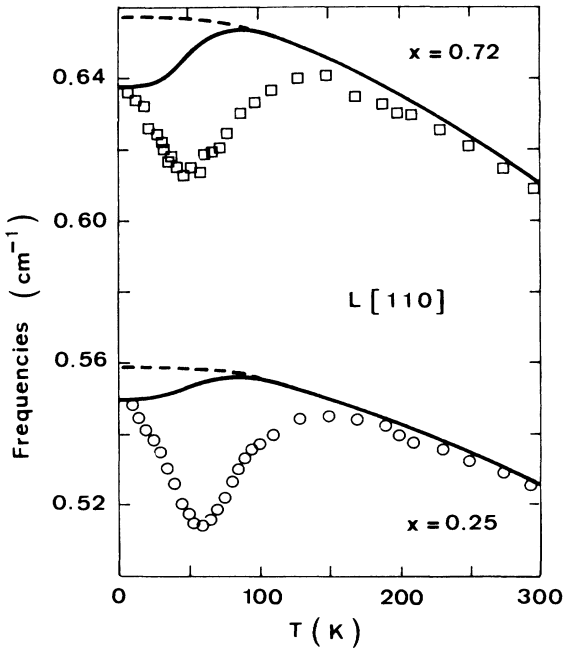

FIG. 13. Frequencies of the LA phonons for $x=0.25$ (lower part) and 0.72 (upper part). The points are the values ω_B from Lorentzian fits to the Brillouin spectra. The dashed curves illustrate the low-temperature extrapolation of the bare frequencies from Fig. 8. The solid curves are the values of ω_a corrected for the static contributions of electrostriction.

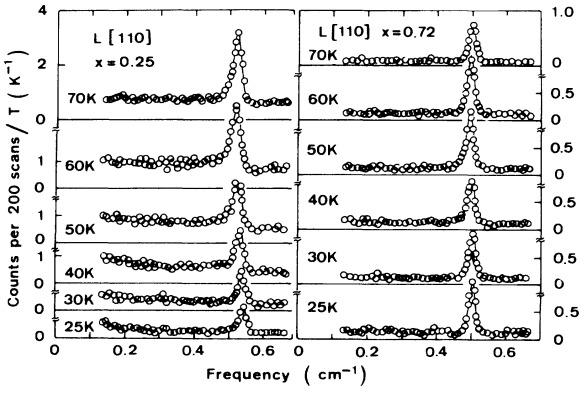

FIG. 14. $L[110]$ spectra for $x=0.25$ (left) and 0.72 (right). The points are the measured values, while the solid lines are fits as explained in the text. Results are presented at the same temperatures and with the same vertical scales for both concentrations, for ease of comparison. On the Rb-rich side, one notices a high background of polarization fluctuations, the wing of a dynamical central peak, and a resonant structure on the high-frequency side of the phonon line. All these features are rather absent on the NH_4-rich side.

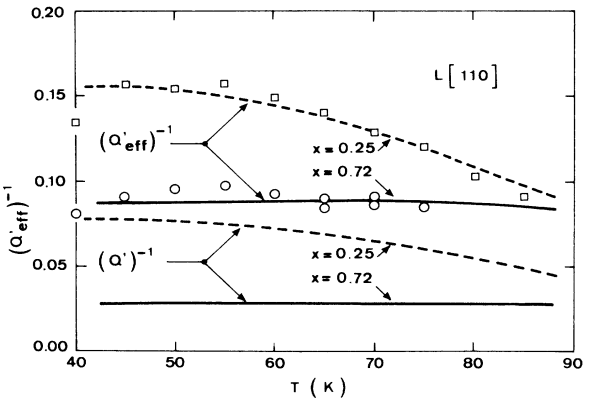

FIG. 15. Inverse of the coupling constant Q for the LA-phonon measurements at $x=0.25$ and 0.72. The lower two curves are calculated from the dielectric measurements, taking into account the different elastic constants of the LA and TA phonons. The points are the result of fits, as explained in the text. The curves through these points, marked $(Q'_{\text{eff}})^{-1}$, are equal to the lower curves multiplied by a constant factor. That this factor is larger for $x=0.72$ indicates a larger contribution of electrostriction at higher NH_4 concentrations.

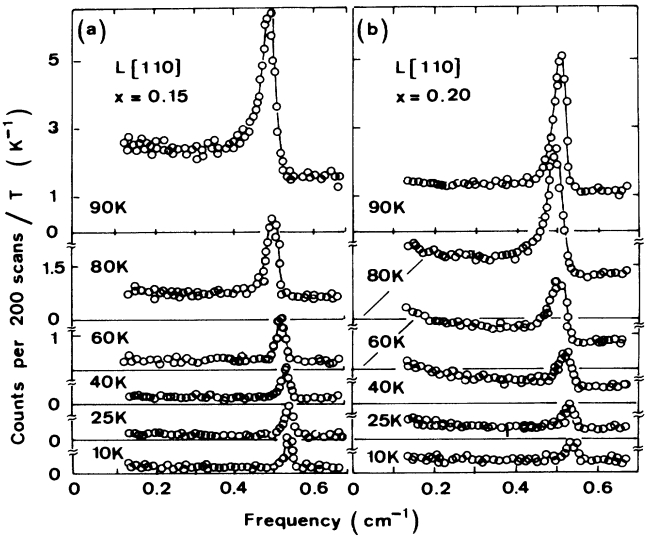

FIG. 16. L[110] spectra for $x=0.15$ (left) and 0.20 (right). The scales are the same as in Fig. 14. The lines are best fits. The very large polarization fluctuations seen for $x=0.15$ quickly disappear on cooling below the phase transition. This is not so for $x=0.20$, as commented on more extensively in the text.

V. OBSERVATIONS OF TRANSITIONS

At concentrations below $x\simeq 0.22$, or above $x\simeq 0.74$, on cooling, scattering attributed to domain walls is observed either in the near-forward direction, or at 90°, below certain temperatures. It was recently found by diffuse x-ray scattering that a tendency to form incommensurate structures I exists near the FE-phase boundary.[8] Accordingly, one can expect a PE-I transition at T_I, and possibly an I-FE once at T_{FE}, where changes in dielectric behavior and/or domain formation could occur.

At $x=0.15$, the dielectric data suggest two successive transitions with $T_I\simeq 92$ K, and $T_{\text{FE}}\simeq 86$ K. The TA phonon softens strongly, from $\simeq 0.14$ cm^{-1} at 110 K to $\simeq 0.07$ cm^{-1} at 95 K, below which its frequency remained almost constant on first cooling. TA measurements could be performed down to $\simeq 92$ K, below which a reflected beam at 90° prevented the measurement. In fact, strong elastically scattered light, unresolved in our experiment, was seen to increase already below $\simeq 97$ K. This "central peak" (CP) is distinct from the *quasielastic* one, already noted in I and II, and whose tail is clearly visible in some of the spectra presented here, such as LA, $x=0.20$, between 80 and 40 K [Fig. 16(b)]. The elastic component grew from 97 K down to 92 K. Its intensity, which was obtained by summing the counts over 21 channels about $\omega=0$, was approximately $\propto(T-91)^{-2}$. This behavior parallels that of elastic CP's observed in other materials undergoing structural phase transitions, in particular KDP.[15] Different behavior was observed on subsequent coolings, with the appearance of diffuse quasielastic spots already at $\simeq 96$ K, and alternation of phonon softening and hardening between 96 and 92 K. This suggests that intermediate phases can be formed. These observations suggest that couplings to strains can play a considerable role in the transitions. The difference of behavior between first and subsequent coolings can well be due to the development of lattice defects able to release internal strains without producing visible damage of the crystal.

In the LA-measurement geometry, domain-wall scattering does not occur in the 90° direction. Hence, spectra could be taken down to liquid-He temperatures. Such spectra are illustrated in Fig. 16(a). On cooling, no anomalies on the LA phonon could be seen around 92 K, but a sudden hardening occurred at $\simeq 85$ K. However, the elastic CP showed a first maximum at 92 K followed by a strong increase at 86 K. We associate these two events with the two peaks in the low-frequency dielectric data [Fig. 1(a)]. The tentative explanation of these observations, in view of the x-ray diffraction results,[8] is that one or several intermediate phases can occur between $\simeq 92$ and $\simeq 85$ K, at which point the material becomes essentially FE. In the intermediate phase [90 K on Fig. 16(a)], very strong polarization fluctuations remain as indicated by the broad and intense frequency-dependent background. This signal is considerably reduced below 85 K, and becomes negligible below 40 K. This indicates that the polarization progressively orders in the FE phase.

For $x=0.20$, in the TA geometry, one observes weak diffuse scattering spots in the forward and backward directions appearing at $\simeq 90$ K. On reaching 58 K, a strong reflection at 90° suddenly appears, suggesting the formation of FE domain walls. On heating back, that reflection disappears at $\simeq 70$ K. This corresponds to the range of the hysteresis in Fig. 1. The TA-phonon frequency softened down to $\simeq 90$ K, where it became approximately constant while, as for the $x=0.15$ sample, the elastic CP intensity continued to increase on cooling with $I\propto(T-70)^{-2}$, saturating around 72 K. This suggests the occurrence of an intermediate phase between $\simeq 90$ and

$\simeq 58$ K on cooling. This change of behavior can be related to the inflection point occurring on the ϵ_c' curve at 10 MHz at $\simeq 90$ K. In view of recent diffuse x-ray scattering results,[8] this inflection could well be related to the onset of incommensurate ordering removing part of the dielectric response at $q=0$.

LA scattering can be measured down to liquid-He temperatures [Fig. 16(b)]. The polarization fluctuations are broad and strong at 90 K, and remain relatively strong down to the lowest temperature (10 K) suggesting that the "ordered-FE" phase (below 58 K) still contains considerable disordered polarization. One notices in particular the *inelastic* CP, already mentioned above, but whose integrated intensity is orders of magnitude smaller than the *elastic* CP seen on the TA mode. This difference of behavior between the $x=0.15$ and 0.20 samples below their respective transitions is remarkable.

Since Q and ω_a of the TA modes are known reliably, at temperatures above the first transition anomalies, the corresponding spectra could be fitted using the approach of II. For $x=0.15$, one finds essentially that $\kappa_R \simeq 1$, with a small decrease down to $\simeq 95$ K, while κ_I slightly increases above 0. This indicates that the relaxation times are shorter than $1/\bar{\omega}$. In this case, the spectra can well be fitted with a single Debye relaxation. For $x=0.20$, the fits could be extended down to $\simeq 70$ K. Then, one notices an onset of relaxational dispersion, less developed than in Fig. 11, but nevertheless evident below $\simeq 80$ K. This suggests a continuity of behavior across the whole concentration range, the observation of a well-developed broad relaxation-time distribution being only prevented by the occurrence of a transition.

On the AFE side, both the $x=0.75$ and $x=0.78$ samples make clear transitions in the ϵ_c' measurement (Fig. 2). They are also seen in light scattering. The TA spectra for $x=0.75$ and 0.78 are weakly coupled to polarization fluctuations, just as for $x=0.72$. This leads to a modest softening of the phonon, as in Fig. 5, and to a small broadening of the Lorentzian profile below the temperature of the minimum velocity. For $x=0.75$, the concentration is apparently extremely close to the limit value for glass formation. The precise transition temperature then becomes strongly sample dependent. It occurs around 40 K for the sample used for TA measurements. At that temperature, the TA phonon starts hardening rapidly on cooling [much faster than in the case of Fig. 5(a)]. On first cooling, although an increase of elastic intensity was observed around 40 K, measurements could be taken down to 10 K. On subsequent coolings, elastic light prevented measurements below 42 K. At $x=0.78$, no TA measurements were possible below the transition at $T \simeq 64$ K. Domain observations indicated a hysteresis of up to 8 K.

As for measurements on the Rb-rich side, the LA phonon could be observed down to liquid-He temperatures in both cases. The frequencies are shown in Fig. 17. At $x=0.75$, near-forward scattering from domains clearly appeared below $\simeq 38$ K in the form of streaks bisecting the z and x directions. At $x=0.78$, a sudden interruption of the high-temperature behavior, followed by a leveling of the LA-phonon frequency, are clearly seen in Fig. 17.

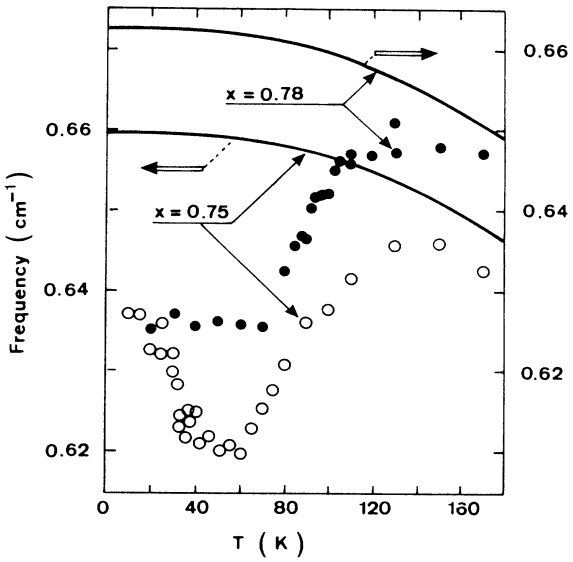

FIG. 17. LA-phonon frequencies for the two highest NH_4 concentrations. The points are the values of ω_B from Lorentzian fits. The solid curves are the fitted ω_a's from Fig. 8. The left scale applies to $x=0.75$ and the right one to $x=0.78$.

VI. SUMMARY AND CONCLUSIONS

The main purpose of this study was to clarify the concentration dependence of the relaxational behavior of RADP at GHz frequencies. This could be achieved from Brillouin-scattering measurements of modes coupled linearly to polarization. Combining the light-scattering results with other data, such as those obtained from dielectric and birefringence measurements, one is able to extract a number of temperature-dependent parameters related to the distribution of relaxation times. Evidence is given that, at sufficiently low temperatures, the distributions acquire considerable weight at times longer than the inverse of the Brillouin frequency. In terms of a Vogel-Fulcher hypothesis, the parameters can be consistently interpreted. This reveals distributions of activation energies which have a greater spread towards Rb-rich samples. It can be understood qualitatively in terms of the nature and size of the clusters that play the dominant role for those relaxations.

We also found that the quadratic coupling of the longitudinal acoustic modes with polarization fluctuations via electrostriction has a considerable effect on the mode frequencies. It increases with NH_4 content, and becomes the major mode-softening mechanism close to the AFE phase boundary. In addition, electrostriction produces a static shift of the bare acoustic frequencies, proportional to the square of local polarizations. Although the dynamic coupling always produces a softening, the static effect can have either sign, depending on the specific values of the electrostriction coefficients discussed in I. We have shown here that the latter contribution to the bare frequency ω_a of the $L[110]$ phonon is negative. Measure-

ments we performed on the $L[001]$ phonon, not reported here, revealed a positive contribution in that case. The sign of these contributions can be related to that of the anomalous low-temperature departures Δa and Δc of the lattice parameters $a(T)$ and $c(T)$ from their Debye behavior.[7,14] As Δa is positive, this dilation makes the lattice softer in the **a** direction, leading to an anomalous $L[110]$ softening. Similarly, the contraction Δc leads to a $L[001]$ hardening.

For crystals undergoing phase transitions, the scattering measurements turned out to be a sensitive test for the appearance of domains. They also revealed possible pretransitional phenomena in terms of growth of elastic central peaks. The measurement of the $L[110]$ frequency could be pursued in the low-temperature phases at all concentrations, and it revealed considerable polarization fluctuations at temperatures below those of the appearance of domains in the case of the $x=0.20$ sample.

In conclusion, this study revealed that Brillouin scattering in structural glasses can provide considerable information, but that its correct interpretation requires a high degree of sophistication. Just as for other transitions, when the freezing is well developed, it is not valid to interpret frequency shifts in terms of linear couplings only. It would also be erroneous to derive frequency-dependent freezing temperatures merely from the position of the minima in plots such as those of Figs. 5 and 13, as one can easily discover. The great advantage of RADP glasses is that quantities of the same tensorial order are accessible both in light scattering and in other measurements. In particular, it has been possible to obtain the important coupling constant Q from dielectric data, and to use it for the interpretation of the Brillouin spectra.

ACKNOWLEDGMENTS

Many thanks are expressed to M. Margot for his expert technical assistance. The Laboratoire de Science des Matériaux Vitreux is associated with the Centre National de la Recherche Scientifique (No. 1119).

*Permanent address: Laboratoire de Science des Matériaux Vitreux, Université de Montpellier II, F-34060 Montpellier, France.

†Present address: 23 av. Général de Gaulle, F-72000 Le Mans, France.

[1]Eric Courtens, J. Phys. (Paris) Lett. **43**, L-199 (1982).

[2]Proceedings of the Sixth International Meeting on Ferroelectricity, Sessions A8 and P18 [Jpn. J. Appl. Phys. **24**, Suppl. 24-2 (1985)].

[3]Eric Courtens and Hans Vogt, Z. Phys. B **62**, 143 (1986); Eric Courtens, Phys. Rev. B **33**, 2975 (1986).

[4]*Landolt-Börnstein, New Series,* Vol. III/16b, edited by K.-H. Hellwege (Springer, Berlin, 1982), pp. 83–95.

[5]E. Courtens and H. Vogt, J. Chim. Phys. (Paris) **82**, 317 (1985); V. H. Schmidt, J. T. Wang, and P. Schnackenberg, in Ref. 2, p. 944; W. Selke and E. Courtens, Ferroelectrics Lett. **5**, 173 (1986); R. A. Cowley, T. W. Ryan, and E. Courtens, Z. Phys. B **65**, 181 (1986).

[6]Eric Courtens, in Ref. 2, p. 70.

[7]Eric Courtens, T. F. Rosenbaum, S. E. Nagler, and P. M. Horn, Phys. Rev. B **29**, 515 (1984).

[8]S. Amin, R. A. Cowley, and E. Courtens, Z. Phys. B (to be published).

[9]E. M. Brody and H. Z. Cummins, Phys. Rev. B **9**, 1979 (1974).

[10]Eric Courtens, René Vacher, and Yves Dagorn, Phys. Rev. B **33**, 7625 (1986).

[11]Eric Courtens and René Vacher, Phys. Rev. B **35**, 7271 (1987).

[12]Eric Courtens, François Huard, and René Vacher, Phys. Rev. Lett. **55**, 722 (1985).

[13]M. Takashige, H. Terauchi, Y. Miura, S. Hoshino, and T. Nakamura, in Ref. 2, p. 947.

[14]H. Terauchi, in Ref. 2, p. 75.

[15]N. Lagakos and H. Z. Cummins, Phys. Rev. B **10**, 1063 (1974); Eric Courtens, Phys. Rev. Lett. **41**, 1171 (1978).